

Light Meson Form Factors from Deep Exclusive Meson Production in early EIC science configurations with the ePIC Detector

G.M. Huber¹, S.J.D. Kay², and L. Preet¹

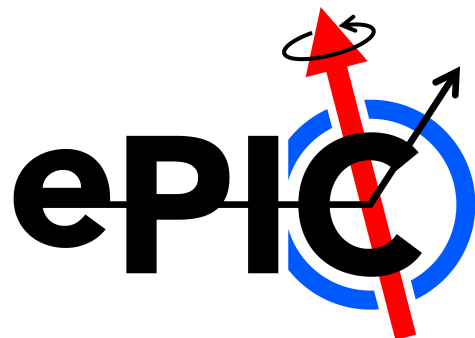
¹Department of Physics, University of Regina, SK, S4S 0A2,
Canada

²School of Physics, Engineering and Technology University of
York, YO10 5DD, UK

MONTH 2025

Abstract

Abstract goes here



Contents

1	Introduction	1
2	Simulation Overview	2
2.1	Event Generator Details	2
3	Event Selection	3
3.1	Event Selection - Identifying Charged Particles	5
3.2	Event Selection - Identifying Neutrons	6
3.3	Event Selection - Calculate Kinematics	6
3.4	Event Selection - Final Cuts	8
3.5	Analysis Code	11
4	Results and Discussion	12
A	Appendix	13

1 Introduction

Pions and kaons are among the most prominent strongly interacting particles next to the nucleon, since they are the Goldstone bosons of QCD. Thus, it is important to study their internal structure and how this reflects their Goldstone boson nature; a question particularly relevant for understanding the origin of mass generation in QCD.

The hard contribution to the π^+ form factor can be calculated exactly within the framework of pQCD, and at asymptotically high Q^2 it takes a particularly simple form, $F_\pi(Q^2) \xrightarrow{Q^2 \rightarrow \infty} 16\pi\alpha_s(Q^2)f_\pi^2/Q^2$ [1], where f_π is the π^+ decay constant. In general, the pion also contains soft contributions, which are expected to dominate at lower Q^2 . The actual behavior of F_π as a function of Q^2 , as QCD transitions smoothly from the non-perturbative (long-distance scale) confinement regime to the perturbative (short-distance scale) regime, is an important test of our understanding of QCD in bound hadron systems. Since QCD calculations cannot yet be performed rigorously in the confinement regime, experimental data from JLab play a vital role in validating the theoretical approaches employed. In particular, due to the charged pion's relatively simple quark-antiquark ($q\bar{q}$) valence structure and its experimental accessibility, the pion elastic form factor (F_π) offers our best hope of directly observing QCD's transition from color-confinement at long distance scales to asymptotic freedom at short distances. It is worth highlighting that in QCD the difference between the kaon and pion charge form factors is of the scale of 20% at $Q^2 \sim 5$ GeV 2 [2] and disappears at asymptotic Q^2 as $\ln(Q^2)$. Thus, the acquisition of experimental data for both form factors covering a wide Q^2 range should be a high priority.

Current experimental information on the pion and kaon form factors is limited, particularly at large Q^2 [3]. Measurement of the π^+ electromagnetic form factor for $Q^2 > 0.3$ GeV 2 can be accomplished by the detection of the exclusive reaction $p(e, e'\pi^+)n$ at low $-t$. This is best described as quasi-elastic (t -channel) scattering of the electron from the virtual π^+ cloud of the proton, where $t = (p_p - p_n)^2$ is the Mandelstam momentum transfer to the target nucleon. Scattering from the π^+ cloud dominates the longitudinal photon cross section ($d\sigma_L/dt$), when $|t| \ll m_p^2$. To reduce background contributions, one preferably separates the components of the cross section due to longitudinal (L) and transverse (T) virtual photons (and the LT, TT interference contributions), via a Rosenbluth separation.

A Rosenbluth separation involves the absolute subtraction of two mea-

surements determined at high- and low-virtual photon polarization (ϵ_{Hi} , ϵ_{Lo}), corresponding to high and low electron beam energies, with very different detector rates. The resulting errors on σ_L and σ_T are magnified by $1/\delta\epsilon = (\epsilon_{Hi} - \epsilon_{Lo})^{-1}$. To keep the uncertainties in σ_L to an acceptable level, $\delta\epsilon > 0.2$ is typically required, *i.e.* an uncertainty magnification of no more than 5. The measurements require continuous, high intensity electron beams, and detectors with good particle identification and reproducible systematics. JLab Hall C is currently the only facility worldwide capable of such studies.

At the EIC, π^+ form factor measurements can be extended to significantly larger Q^2 than possible at JLab. We have written an exclusive $p(e, e'\pi^+n)$ event generator [4] and performed detailed simulations to determine the feasibility of F_π measurements at the EIC. The key questions we have addressed include: 1) detector requirements to cleanly identify exclusive $e'\pi^+n$ coincidences; 2) experimental acceptance and projected counting rates for such triple coincidences; 3) event reconstruction resolution requirements to reliably extract $F_\pi(Q^2)$ from $p(e, e'\pi^+n)$ data. Since the cross section falls rapidly as the distance from the pion pole ($t - m_\pi^2$) is increased, this steep fall off needs to be measured to confirm the dominance of the pion cloud mechanism in the acquired data. This note describes our work addressing all of these questions and evaluating what can be achieved with the EIC in its first five years of running.

2 Simulation Overview

The analysis presented in this note utilises our event generator, DEMPgen [4], in conjunction with the ePIC software stack to produce projections for pion form factor measurements at the EIC. Details on the event generator, simulation and subsequent reconstruction are presented in this section.

2.1 Event Generator Details

DEMPgen version 1.2.4¹ was utilised to generate $p(e, e'\pi^+n)$ events for this study. DEMPgen events are absolutely-normalized so that project event rates can easily be predicted. This normalization is maintained in the form of an event weighting which is retained through the simulation and reconstruction

¹<https://github.com/JeffersonLab/DEMPgen/releases>

chain before being applied to final results. Two different early science configurations were studied, namely 10 GeV electron on 130 GeV (10x130) proton and 10 GeV electron on 250 GeV proton (10x250) collisions. Events were generated over the following kinematic range:

- $5 < Q^2 < 35$
- $-t < 0.45$
- $2 < W < 10.2$

For each beam energy, events were generated in three distinct Q^2 ranges to ensure adequate simulated statistics in each region. These three regions were:

- $5 < Q^2 < 10$
- $10 < Q^2 < 20$
- $20 < Q^2 < 35$

Four hundred thousand events were generated in each Q^2 range for each beam energy combination. Each Q^2 region was selected by imposing a cut on the generation range of scattered electron energies when running the event generator. The resulting output hepmc3 files produced by the generator were processed through the EIC afterburner [5] to apply beam effects. The resulting files were then passed to the ePIC production working group for processing as part of monthly simulation campaigns. Details on how to reproduce the files provided to the production working group, including all simulation input .json cards, can be found here.².

3 Event Selection

DEMP $p(e, e'\pi^+n)$ events have very well defined kinematics. The scattered electron, e' and produced meson, π^+ , are detected by the electron or hadron end caps respectively in most cases, with some events ending up in the central

²https://github.com/JeffersonLab/DEMPgen/tree/develop/Jul2025_ePIC_Simulation_Campaign

barrel. The neutrons carry the majority of the initial proton beam momentum and as such, are detected in the far forward detectors, primarily the ZDC. The distribution of events for 10x130 and 10x250 events can be seen in Figs. 1 and 2 below.

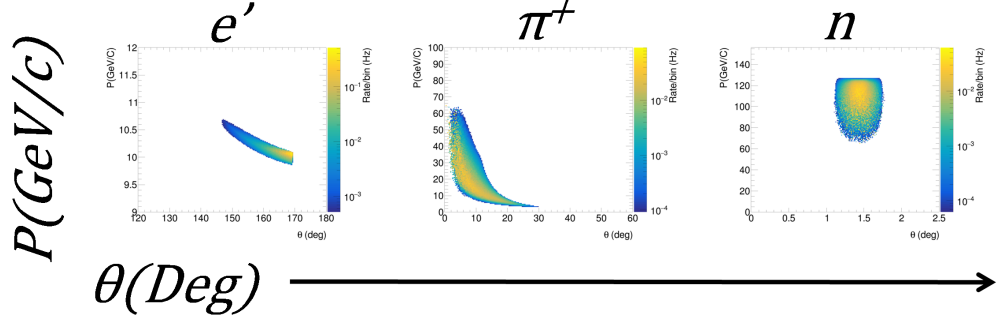


Figure 1: Momentum and polar angle (θ) distribution of scattered electrons, e' , pions, π^+ and neutrons, n for 10x130 events. Note that the z scale is a rate in Hz due to the absolute normalisation of DEMPgen.

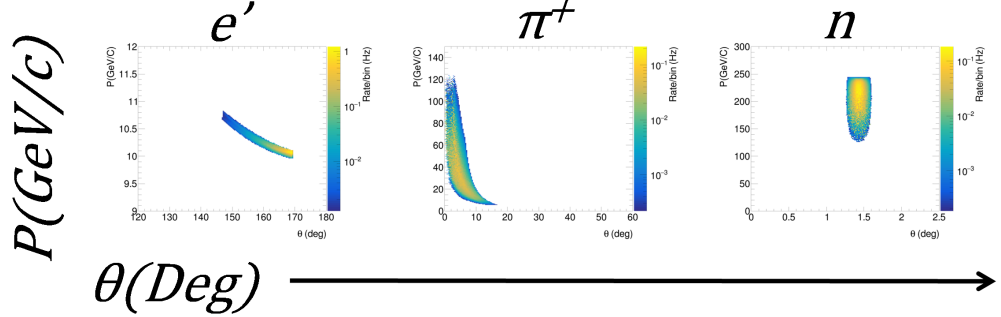


Figure 2: Momentum and polar angle (θ) distribution of scattered electrons, e' , pions, π^+ and neutrons, n for 10x250 events. Note that the z scale is a rate in Hz due to the absolute normalisation of DEMPgen.

This makes the event selection process relatively straightforward with a clearly defined sequence:

1. Identify charged particles (e' and π^+)

2. Identify neutrons incident on the ZDC
3. Calculate kinematics
4. Apply exclusivity and other cuts

Each stage has some cuts applied which are detailed below.

3.1 Event Selection - Identifying Charged Particles

Due to the distribution of particles in DEMP $p(e, e'\pi^+n)$ events, selection of charged particles are very straightforward. The method to identify the scattered electron is based upon the EIC electron finder [6], but is coded in a different style. To identify the scattered electron, the analysis code searches for the highest energy cluster in the barrel electromagnetic calorimeter or the end cap (electron direction) electromagnetic calorimeter. Specifically, the branches “EcalEndcapNClusters” and “EcalBarrelClusters” within EICrecon are searched. The code then checks that the energy of this cluster is $> 0.8*E_{eBeam}$, if it is lower, the event is discarded. If the cluster is in the barrel, the code also checks that this cluster is in the negative z side (electron going direction) of the calorimeter. Again, if this condition is not met, the event is discarded. This step is staggered such that first the end cap is checked for a good cluster, if none is found, the barrel is then searched.

If a “good” cluster is identified for an event, the code then checks the “ReconstructedChargedParticles” for a track. The code searches for a track with a negative charge, with the track momentum in the $-z$ direction. There is also a requirement that this track has $|\vec{P}|$ greater than 80% of the incident electron beam energy, $8 \text{ GeV}/c$ in both beam energy combinations studied in this note. Once a good track and good cluster have been identified, the code then calculates the momentum, P , from a combination of the track and cluster information. This is used to calculate an E/P value for the track plus cluster combination. For real electron signals, this value should be close to ~ 1 . As such, a cut is applied on this value and only events with $0.8 < E/P < 1.2$ are retained. If this condition is passed, the track information **only** is assigned to the e' for this event. Calorimeter information is only utilised to veto events and is not used in subsequent calculations.

Note that there is a gap in acceptance between the barrel and end cap calorimeters approximately between $160^\circ < \theta < 163^\circ$. If no calorimeter cluster is found matching the initial criteria, but a track that passes the

selection cuts above is identified with θ in this range, the track information is assigned to the e' for this event still. This is to compensate for the fact that due to the lack of calorimeter coverage in this region, we cannot expect to see a cluster for these tracks.

Pion selection currently utilises a slightly simpler approach. The pion is identified by selecting a reconstructed charged particle track with a positive charge and with the track momentum in the $+z$ direction. There is also a requirement that this track has $|\vec{P}|$ greater than $1\text{ GeV}/c$. This requirement is included to remove any low momentum noise/background events that may be present.

3.2 Event Selection - Identifying Neutrons

For the beam energy combinations studied, the neutron produced in this reaction is incident on, and detected in, the ZDC in almost all generated events. As such, neutron identification is straightforward. Neutrons are identified from the “ReconstructedFarForwardZDCNeutrals” EICrecon branch. To filter out events that are not incident upon the ZDC and to remove low energy events, cuts are implemented on θ^* and the reconstructed neutral particle energy. θ^* is the polar angle θ after a rotation of 25 mRad around the proton beam axis to remove the effect of the beam crossing angle. After this rotation, the ZDC is indeed, centred at roughly “zero degrees”. A cut of $\theta^* < 4\text{ mRad}$ is applied. To remove low energy hits, a cut-off of the neutral particle energy being greater than 40 GeV is applied for 10×130 events. For 10×250 events, this cut off is increased to 120 GeV .

3.3 Event Selection - Calculate Kinematics

Before calculating any kinematic quantities such as Q^2 and $-t$, the analysis code requires that a candidate e' , π^+ and n that pass relevant selection cuts (as defined above) have been found in coincidence. If this condition is met, the code calculates Q^2 , the negative four-momentum transfer squared at the electron vertex. Q^2 can be calculated using various different methods as discussed here³. For the kinematic region under investigation in this study, the double angle, DA, method proved to be optimal as seen in Fig .3. It

³https://agenda.infn.it/event/43344/contributions/253198/attachments/130672/194493/EIC_KinematicReconstruction.pdf

is apparent that this calculation method closely matches the “true” value across the relevant Q^2 range (5 to 35) as seen in Fig. 4. Once calculated, a cut on Q_{DA}^2 being within 5 and 35 (GeV/c^2)² is applied.

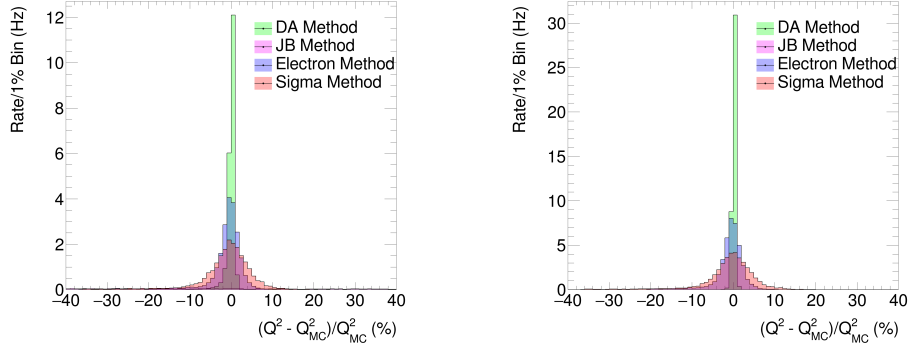


Figure 3: A comparison of the resolution for calculated Q^2 values, defined as the deviation from the MC truth divided by the MC truth value and expressed as a percentage, for 10x130 (left) and 10x250 (right) event samples. Q_{DA}^2 is clearly the most accurate in both cases, note that it is clear that the JB method is not applicable in DEMP kinematics. The distribution for this extends beyond the range of the plot quite significantly.

Once events outside the relevant Q^2 range are removed, further kinematic quantities are calculated. The squared four-momentum transfer between the initial (p) and final (n) hadron state, $-t$, is critical to determine accurately for DEMP studies. Measurements are needed at the lowest $-t$ possible in order to get as close to the pion pole as possible. As with Q^2 , there are many ways to determine $-t$. These are defined in the *tRECO* convention document need a link/reference/citation for this! If none, add relevant text for the calculation. Link to generic code etc.. DEMP can utilise the t_{eXBABE} method which exploits the exclusive nature of the reaction to “correct” the measured neutron track. This method outperforms any reconstruction methods as can be seen in Fig. 5. This determination of $-t$ also strongly correlates with the MC truth value of $-t$ as can be seen in Fig. 6.

Once calculated, a cut is applied on $-t$. Any events with $0 < -t_{eXBABE} < 1.4 (GeV/c)^2$ are removed. A cut on $W > 0 GeV$ is also applied with any events failing this selection being removed. These cuts are applied simultaneously in conjunction with other cuts that are described in Sec. 3.4.

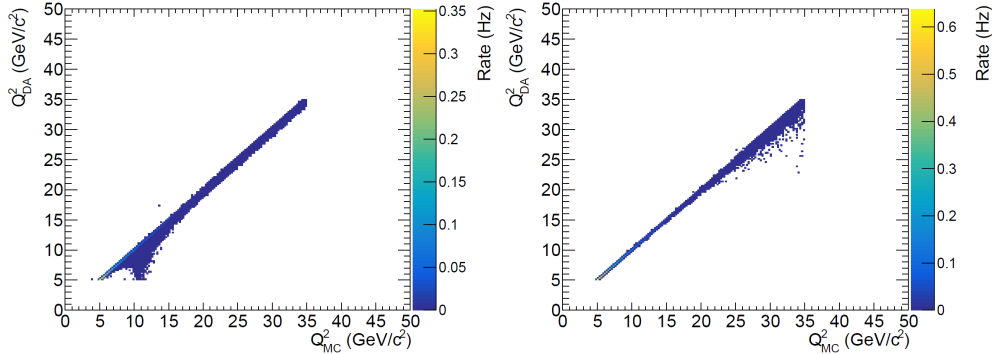


Figure 4: A comparison of Q_{DA}^2 against the MC truth value of Q^2 for 10x130 (left) and 10x250 (right) event samples.

3.4 Event Selection - Final Cuts

To ensure exclusivity and remove background events, further cuts are needed. This DEMP analysis utilises a somewhat unique cut to achieve these objectives. To implement this cut, a missing momentum vector is determined from the reconstructed e' and π^+ tracks -

$$\vec{P}_{nMiss} = (\vec{e} + \vec{p}) - (\vec{e'}_{Rec} + \vec{\pi}_{Rec})$$

where \vec{e} and \vec{p} are the initial electron and proton beam 4-vectors. If this is an exclusive event, the resulting four vector should correspond to the neutron, hence P_{nMiss} . The polar and azimuthal (θ_{nMiss}^* and ϕ_{nMiss}^*) angles of this track (after rotation by 25 mRad to remove beam crossing effects) should correspond to the polar and azimuthal angles determined from the neutron hit on the ZDC (θ_{ZDC}^* and ϕ_{ZDC}^* , again, after rotation by 25 mRad). Two differences, $\Delta\theta^*a$ and $\Delta\phi^*i$ can then be defined and calculated as -

$$\begin{aligned}\Delta\theta^* &= \theta_{nMiss}^* - \theta_{ZDC}^*, \\ \Delta\phi^* &= \phi_{nMiss}^* - \phi_{ZDC}^*.\end{aligned}$$

For exclusive events, these differences should be very small, particularly $\Delta\theta^*$ due to the excellent position resolution of the ZDC. As such, only events satisfying -

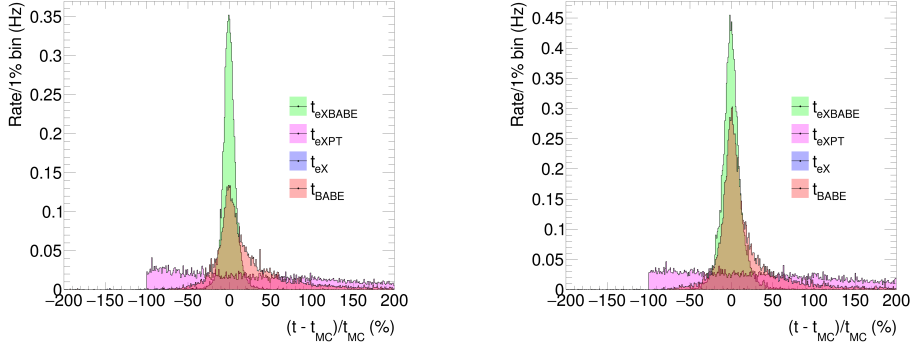


Figure 5: A comparison of the resolution for calculated $-t$ values, defined as the deviation from the MC truth divided by the MC truth value and expressed as a percentage, for 10x130 (left) and 10x250 (right) event samples. t_{eXBABE} is clearly the most accurate determination in each case.

$$\begin{aligned} -0.09^\circ < \Delta\theta^* < 0.14^\circ, \\ -55^\circ < \Delta\phi^* < 55^\circ, \end{aligned}$$

for 10x130 events and

$$\begin{aligned} -0.07^\circ < \Delta\theta^* < 0.17^\circ, \\ -80^\circ < \Delta\phi^* < 80^\circ, \end{aligned}$$

for 10x250 events are retained. These ranges were chosen to fit along lines of constant rate in a plot of $\Delta\theta^*$ vs $\Delta\phi^*$, such as in Fig.7, to ensure no variations across the acceptance of the ZDC. They were also chosen so as to be conservative as SIDIS or other background events, which should not reconstruct in this range, will be excluded. For non-exclusive events, the missing momentum vector should not correspond to a single particle and as such, $\Delta\theta^*$ and $\Delta\phi^*$ should be spread across a much broader range.

This cut is an indirect cut on the missing momentum and, as a consequence, the missing energy. However, to further reduce any potential background events leaking in, a further, direct cut on the missing momentum is applied. The missing momentum for the full DEMP system is calculated as

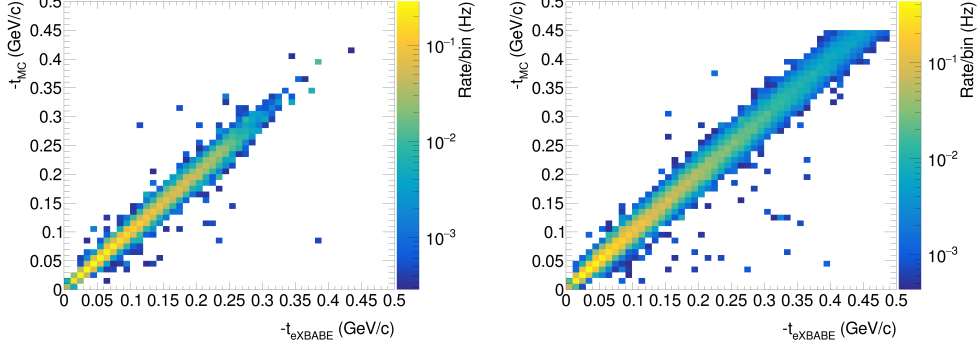


Figure 6: A comparison of $-t_{eXBABE}$ against the MC truth value of $-t$ for 10x130 (left) and 10x250 (right) event samples. Need to update units.

$$\vec{P}_{MDEM} = (\vec{e} + \vec{p}) - (\vec{e} \gamma_{Rec} + \vec{\pi}_{Rec} + \vec{n}_{Rec})$$

Cuts are applied on the $.M2()$ and $.M()$ values of this 4-vector. Events with:

$$\vec{P}_{MDEM}.M2() < -1 \text{ (GeV/c)}^2, \vec{P}_{MDEM}.M() > 0.75 \text{ GeV}/c^2,$$

are removed respectively. This is to account for the fact that for a true exclusive event, all particles in the event should be detected and as such, the “missing” mass should be ≈ 0 .

Add figure with M2 and M distributions showing cuts.

Finally, a cut on the sum of $E - P_z$ for all detected final state particles is applied. In the absence of initial state radiation or background events, this sum should be roughly equal to two times the electron beam energy (20 GeV in each case under study here). As such, a cut of -

$$18 < \sum (E - P_z) < 22,$$

is applied. Again, as no initial state radiation is included in DEMPgen and no background events are included in the event sample, this range has been chosen to be conservative. This cut range will likely be tweaked and adjusted as these effects are incorporated in future studies.

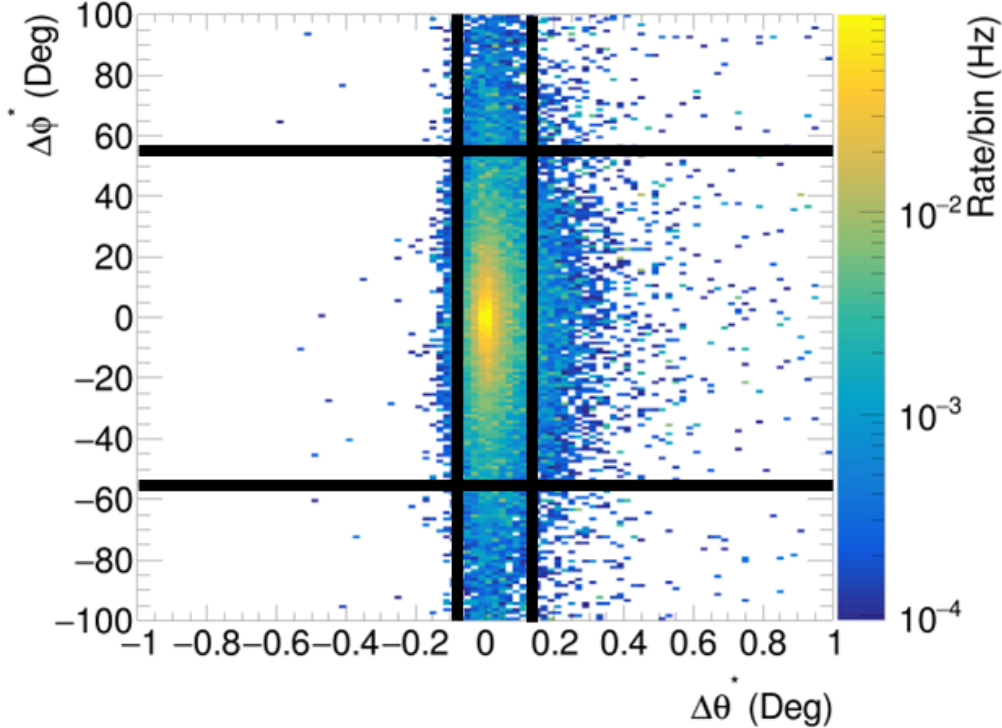


Figure 7: $\Delta\theta^*$ vs $\Delta\phi^*$ for 10x130 events. Note that as only DEMP events are processed, the majority of events survive this cut. Cuts were chosen along lines of constant rate as the peak area of the distribution tails off, as indicated by the solid black lines showing the cut region.

3.5 Analysis Code

The analysis of processed DEMP events is via a standard ROOT/C++ based macro. The analysis code is stored on GitHub and can be accessed here⁴. This repository also contains some utility scripts that can be used to cut down the size of the reconstructed simulation output if desired.

⁴https://github.com/sjdkay/ePIC_DEMP_Analysis/blob/main/DEMP_Analysis.C

4 Results and Discussion

Your results with key performance plots etc. Consult checklist of key figures, see page three of this presentation as an example of plots to include.

Once triple-coincidence $p(e, e'\pi^+n)$ events are cleanly identified with ePIC, the value of $F_\pi(Q^2)$ is determined by comparing the measured $d\sigma/dt$ values at small $-t$ to the best available electroproduction model. The obtained F_π values are in principle dependent upon the model used, but one anticipates this dependence to be reduced at sufficiently small $-t$. Measurements over a range of $-t$ are an essential part of the model validation process. The JLab 6 GeV experiments were instrumental in establishing the reliability of this technique up to $Q^2 = 2.45$ GeV 2 [3, 7–14], and extensive further tests are planned as part of JLab experiment E12-19-006 [15].

GH can add more discussion later.

A Appendix

Material you wish to include in an appendix.

References

- [1] G. Peter Lepage, S. J. Brodsky, Exclusive processes in quantum chromodynamics: Evolution equations for hadronic wavefunctions and the form factors of mesons, Physics Letters B 87 (4) (1979) 359–365.
doi:[https://doi.org/10.1016/0370-2693\(79\)90554-9](https://doi.org/10.1016/0370-2693(79)90554-9).
URL <https://www.sciencedirect.com/science/article/pii/0370269379905549>
- [2] F. Gao, L. Chang, Y.-X. Liu, C. D. Roberts, P. C. Tandy, Exposing strangeness: projections for kaon electromagnetic form factors, Phys. Rev. D 96 (3) (2017) 034024. [arXiv:1703.04875](https://arxiv.org/abs/1703.04875), doi:10.1103/PhysRevD.96.034024.
- [3] T. Horn, C. D. Roberts, The pion: an enigma within the Standard Model, J. Phys. G. 43 (2016) 073001.
- [4] Z. Ahmed, et al., Dempgen: Physics event generator for deep exclusive meson production at jefferson lab and the eic, Computer Physics Communications 308 (2025) 109444.
doi:<https://doi.org/10.1016/j.cpc.2024.109444>.
URL <https://www.sciencedirect.com/science/article/pii/S0010465524003679>
- [5] A. Jentsch, et al., EIC MC afterburner.
URL <https://github.com/eic/afterburner>
- [6] T. Kutz, et al.
- [7] G. Huber, et al., Charged pion form-factor between $Q^2 = 0.60 \text{ GeV}^2$ and 2.45 GeV^2 . II. Determination of, and results for, the pion form-factor, Phys. Rev. C 78 (2008) 045203. [arXiv:0809.3052](https://arxiv.org/abs/0809.3052), doi:10.1103/PhysRevC.78.045203.

- [8] T. Horn, et al., Scaling study of the pion electroproduction cross sections and the pion form factor, Phys. Rev. C 78 (2008) 058201. [arXiv:0707.1794](#), doi:[10.1103/PhysRevC.78.058201](https://doi.org/10.1103/PhysRevC.78.058201).
- [9] J. Volmer, et al., Measurement of the Charged Pion Electromagnetic Form-Factor, Phys. Rev. Lett. 86 (2001) 1713–1716. [arXiv:nucl-ex/0010009](#), doi:[10.1103/PhysRevLett.86.1713](https://doi.org/10.1103/PhysRevLett.86.1713).
- [10] T. Horn, et al., Determination of the Pion Charge Form Factor at $Q^2 = 1.60$ and $2.45 \text{ (GeV}/c)^2$, Phys. Rev. Lett. 97 (2006) 192001. [arXiv:nucl-ex/0607005](#), doi:[10.1103/PhysRevLett.97.192001](https://doi.org/10.1103/PhysRevLett.97.192001).
- [11] V. Tadevosyan, et al., Determination of the pion charge form factor for $Q^2 = 0.60\text{--}1.60 \text{ GeV}^2$, Phys. Rev. C 75 (2007) 055205. [arXiv:nucl-ex/0607007](#), doi:[10.1103/PhysRevC.75.055205](https://doi.org/10.1103/PhysRevC.75.055205).
- [12] H. Blok, et al., Charged pion form factor between $Q^2=0.60$ and 2.45 GeV^2 . I. Measurements of the cross section for the ${}^1\text{H}(e, e'\pi^+)n$ reaction, Phys. Rev. C 78 (2008) 045202. [arXiv:0809.3161](#), doi:[10.1103/PhysRevC.78.045202](https://doi.org/10.1103/PhysRevC.78.045202).
- [13] G. Huber, et al., Separated Response Function Ratios in Exclusive, Forward π^\pm Electroproduction, Phys. Rev. Lett. 112 (18) (2014) 182501. [arXiv:1404.3985](#), doi:[10.1103/PhysRevLett.112.182501](https://doi.org/10.1103/PhysRevLett.112.182501).
- [14] G. Huber, et al., Separated Response Functions in Exclusive, Forward π^\pm Electroproduction on Deuterium, Phys. Rev. C 91 (1) (2015) 015202. [arXiv:1412.5140](#), doi:[10.1103/PhysRevC.91.015202](https://doi.org/10.1103/PhysRevC.91.015202).
- [15] G. M. Huber, D. Gaskell, T. Horn, et al., Measurement of the Charged Pion Form Factor to High Q^2 and Scaling Study of the L/T-Separated Pion Electroproduction Cross Section at 11 GeV, jefferson Lab 12 GeV Experiment E12-19-006.
URL https://www.jlab.org/exp_prog/proposals/19/E12-19-006.pdf